

Article

Thermo-Calc Prediction of Mushy Zone in AlSiFeMn Alloys

Piotr Mikolajczak ^{1,*} , Amber Genau ², Jerzy Janiszewski ³ and Lorenz Ratke ⁴

¹ Institute of Materials Technology, Poznan University of Technology, Piotrowo 3, 60-965 Poznan, Poland

² Department of Materials Science and Engineering, University of Alabama at Birmingham, 1720 2nd Avenue South, Birmingham, AL 35294, USA; Genau@uab.edu

³ Institute of Electrical Power Engineering, Poznan University of Technology, Piotrow 3A, 60-965 Poznan, Poland; Jerzy.Janiszewski@put.poznan.pl

⁴ Institut für Werkstoff-Forschung, German Aerospace Center DLR, Linder Höhe, 51147 Köln, Germany; Lorenz.Ratke@dlr.de

* Correspondence: Piotr.Mikolajczak@put.poznan.pl; Tel.: +48-61-665-2804

Received: 22 October 2017; Accepted: 13 November 2017; Published: 16 November 2017

Abstract: Convection forces can cause significant segregation within the liquid during directional solidification, influencing the structure of the mushy zone and the type and distribution of phases present in the solidified alloy. The solidification behavior of AlSiFeMn alloys with strong convection was investigated via experimental results combined with thermodynamic calculations. Experimental specimens were processed in a directional solidification facility with forced melt flow, resulting in high levels of elemental segregation across samples. The resulting local compositions were located on phase diagrams Al-Si-Fe, Al-Si-Mn and Al-Fe-Mn for prediction of the variation in solidification behavior. Phase mass fraction diagrams created in Thermo-Calc showed the effect of segregation on the characteristic temperatures, mushy zone length and the order of occurring phases precipitating across specimens. These findings were used to create 2D maps for visualization of the mushy zone, mass fraction of α -Al dendrites, β -Al₅FeSi, Al₁₅Si₂Mn₄ and their spatial location. The specimen centers showed enrichment in AlSi-eutectic but for β -Al₅FeSi and Al₁₅Si₂Mn₄ results are ambiguous. Fe-phases start to grow mainly behind the dendrites tips and in general may flow between them. Mn-rich phases start to precipitate at higher temperatures than β and in many places before α -Al and in this way may flow in the melt above the mushy zone.

Keywords: mushy zone; aluminum alloys; directional solidification; Thermo-Calc; Fe- Mn-intermetallics; β -Al₅FeSi; Al₁₅Si₂Mn₄

1. Introduction

The relationship between process conditions, microstructure and composition is an important consideration in the design of industrial processes. Phase diagrams are an important tool correlating these factors in both simple and more complicated materials systems [1]. For predicting the occurrence of phases and the interactions between them [2–5], modeling of thermodynamic properties using the numerical method CALPHAD (Computer Coupling of Phase Diagrams and Thermochemistry) has emerged more recently as another valuable tool.

Aluminum alloys are widely used in a variety of engineering applications, particularly the automotive and aerospace industries. These alloys are characterized by an excellent combination of properties such as low coefficient of thermal expansion, high strength to weight ratio, and in Al-Si alloys good castability. In the microstructure of AlSi alloy, primary grains of α -Al are visible, with interdendritic regions of AlSi eutectic and often minor intermetallic phases resulting from the presence of various impurity elements. The presence of iron most commonly results in β -Al₅FeSi,

with a monoclinic crystal structure, which has a significant negative impact on ductility [6–8]. Beryllium, molybdenum, chromium and manganese have been used to prevent the β phase by tying up the Fe in another phase such as α -Al(Mn, Fe)Si, which has a skeleton (or Chinese script) or granular morphology. One of the most important and effective elements for controlling the Fe-rich intermetallics [9–12] is manganese, so understanding and predicting solidification behavior is of special importance in the Al-Si-Fe-Mn system.

In the current paper, we use directional solidification to experimentally investigate the behavior of several Al-Si-Fe-Mn alloys. Directional solidification [13,14] is a valuable research technique for this type of investigation because it permits precise and independent control of composition, solidification velocity and temperature gradient inside the specimens during freezing. It is used to study e.g., phase selection or crystal growth [15,16]. In addition, we use thermodynamic calculations to estimate the mushy zone length and shape and to predict the precipitation sequence of various phases in AlSi alloys with Fe- and Mn-rich intermetallics. We used Thermo-Calc [17] software for calculation of phase mass fraction diagrams and ternary phase diagrams that enabled us to construct 2D maps of the mushy zone.

2. Materials and Methods

In order to prepare alloy samples, we used high purity elements: Al (99.999%, Hydro Aluminum Deutschland GmbH, Bonn, Germany), Si (Crystal Growth Laboratory, Berlin, Germany), Fe (ferroaluminum 50 wt. % Al-50 wt. % Fe, Goodfellow Cambridge Ltd., Huntingdon, UK) and Mn (from Manganese Flake 99.95%, Goodfellow Cambridge Ltd., Huntingdon, UK). The study considered hypoeutectic aluminum alloys with 0.2, 0.4 and 1.0 wt. % Fe and 0.2, 0.4 and 1.0 wt. % Mn and with 5 wt. % Si. The values of Si, Fe and Mn were chosen to be similar to industrial quality casting alloys. From the given values of silicon, iron and manganese we prepared and processed five samples that allowed analysis of the effect of each element individually on the mushy zone microstructure.

Specimens with 120 mm length and 8 mm diameter were directionally solidified under controlled conditions [18–20] in Bridgman-type furnace Artemis-3 (German Aerospace Center, Cologne, Germany). Specimens were solidified within crucibles made of silica aerogel, and thermal conditions were generated by a lower heater (equipped with an active cooling system) and by upper heater [18,20]. Due to the construction of the cooling system and lower and upper heaters, solidification can proceed with velocity in the range $v = 0.02$ – 0.12 mm/s and with a temperature gradient reaching $G = 3$ K/mm. In order to allow an extended period of melt stirring to affect the mushy zone, specimens were processed with solidification velocity $v = 0.04$ mm/s and a temperature gradient $G = 3$ K/mm. Fluid flow was generated by a rotating magnetic field (RMF) induced through three pairs of coils placed near to the sample. The measured RMF can reach 3 mT or 6 mT at a frequency of 50 Hz. In the current study RMF of 6 mT was chosen, generating stirring with first azimuthal flow and secondary flows in axial and radial directions [21–23], and producing specimens with enrichment of eutectics or intermetallics in the center.

The transverse cross-sections (Figures 1 and 2) were extracted from the middle region of the whole sample at a height of 45 mm (Isocut 4000, Buehler, Lake Bluff, IL, USA) from the lower heater. A solidification distance of 45 mm corresponds to the position where the specimen was cut and to the coordinate 0 mm (Figure 2b) on the longitudinal section. The chemical composition was investigated using EDS (Princeton Gamma-Tech Instruments Inc., Princeton, NJ, USA) in Vega Tescan SEM (Tescan, Brno, Czech Republic) on the cross-sections (Figure 1a). Each EDS measurement was performed at 22 points (Figure 1b) spaced 0.363 mm apart. The composition profiles of silicon, iron and manganese created with EDS (Figure 1b) show some increase toward the center, which is also visible (Figure 1a) as the enrichment in AlSi-eutectic in the specimen center.

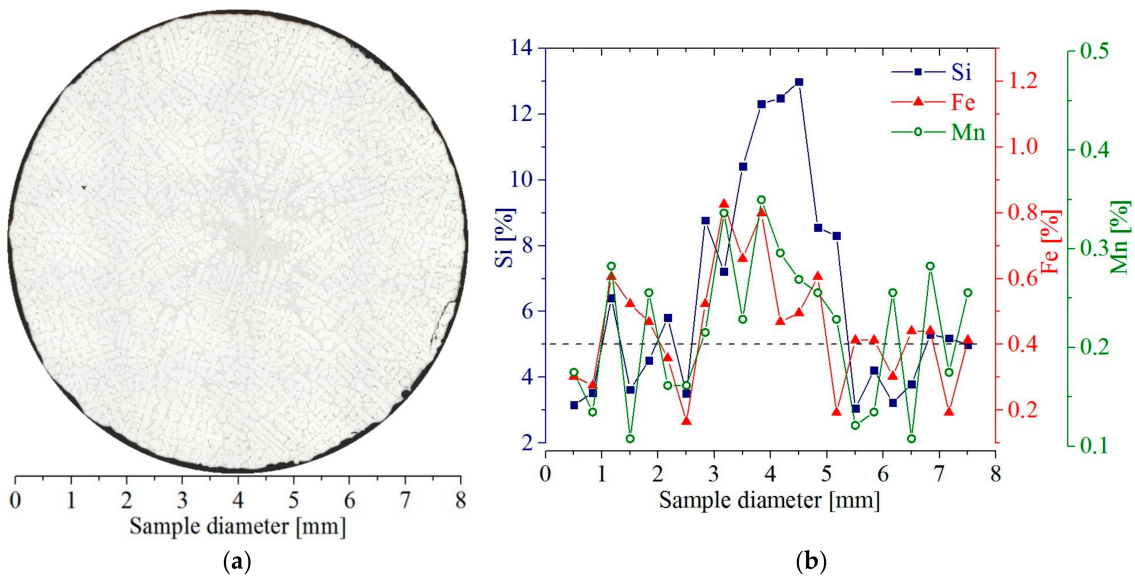


Figure 1. Specimen of Al-5 wt. % Si-0.4 wt. % Fe-0.2 wt. % Mn alloy solidified with temperature gradient $G = 3 \text{ K/mm}$, velocity $v = 0.04 \text{ mm/s}$ and rotating magnetic field $\text{RMF } B = 6 \text{ mT}$: (a) a cross-sectional microstructure; (b) solute concentration profile—Si, Fe and Mn—measured across specimen cross section.

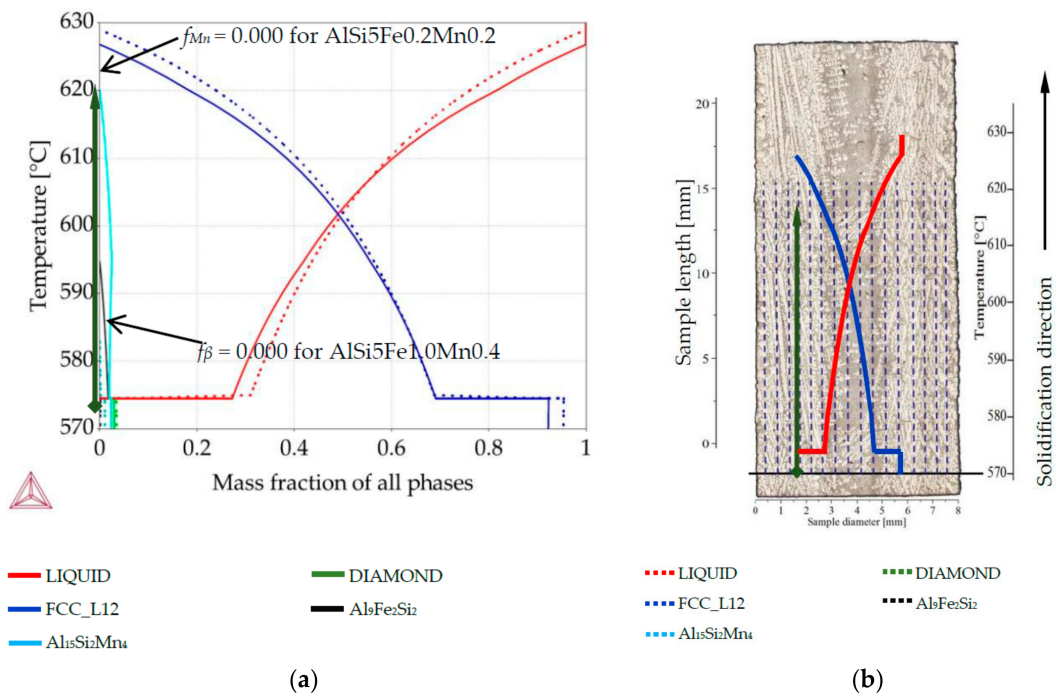


Figure 2. Illustration of phase fraction diagrams application for 2D maps construction. The green arrow and red and blue courses show the connection between property diagram’s temperature axis and longitudinal section’s temperature axis: (a) phase fraction diagram for AlSi5Fe0.2Mn0.2 (solid line) and AlSi5Fe1.0Mn0.4 (dotted line) alloys; (b) longitudinal section with marked sites for mass fraction placement (dashed lines oriented along sample length) and placed mass fraction courses (red and blue).

We have investigated five samples, one for each alloy. The first had composition with nominal values (nominal composition) Al-5 wt. % Si-0.2 wt. % Fe-0.2 wt. % Mn, which we will refer to as AlSi5Fe0.2Mn0.2. Using the same naming convention, the other four samples had nominal compositions AlSi5Fe0.2Mn0.4, AlSi5Fe0.4Mn0.2, AlSi5Fe0.4Mn1.0, and AlSi5Fe1.0Mn0.4. All were solidified with fluid

flow induced by RMF as described above. The transverse cross-sections (Figure 1a) and longitudinal sections (Figure 2b) showed segregation across the diameter as an enrichment in AlSi-eutectic [21,24] and increase in Si, Fe and Mn content (Figure 1b). For each specimens' nominal composition, Thermo-Calc was used to create phase mass fraction diagrams (so-called "property diagrams") (Figure 2a), which show the evolving phase fractions as a function of decreasing temperature for a specific composition. The measured chemical compositions for quaternary alloys were graphed onto three ternary phase diagrams Al-Si-Fe (Figure 3a), Al-Si-Mn (Figure 3b) and Al-Fe-Mn (Figure 4) and were considered as independent alloys solidifying in specific areas inside each specimen. All calculations were done with Thermo-Calc 4.1 [17] software and databases TCAI3 (TCS Al-based alloys database v.3) and MOBAI3 (TCS Al-alloys mobility database v.3) were applied.

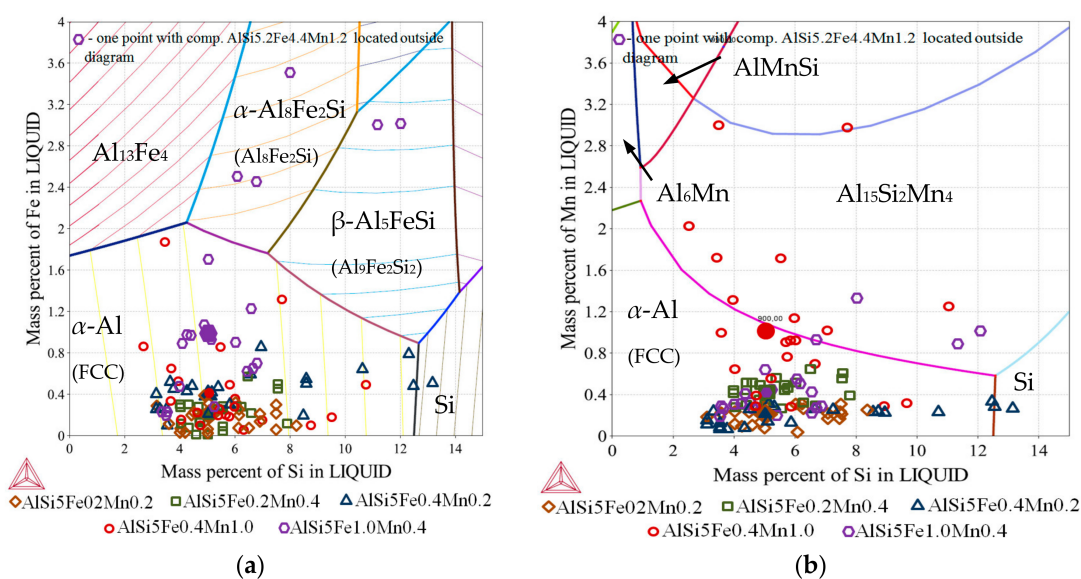


Figure 3. Phase diagrams: (a) Liquidus projection of Al-Si-Fe system with plotted EDS measured chemical compositions (in selected 22 points as on Figure 1); (b) Liquidus projection of Al-Si-Mn system with plotted EDS measured chemical compositions (in selected 22 points as on Figure 1).

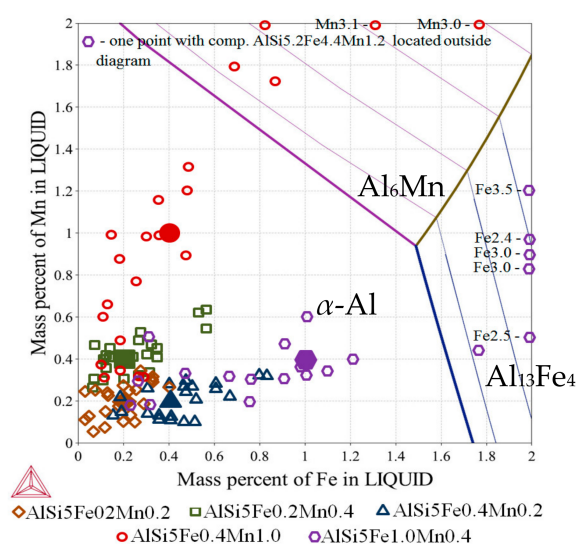


Figure 4. Phase diagram. Liquidus projection of Al-Fe-Mn system with plotted EDS measured chemical compositions (in selected 22 points as on Figure 1).

From the 22 chemical compositions recorded across the diameter of each specimen (Figure 1b), two compositions per sample were selected. For those compositions, Thermo-Calc was used to create phase fraction diagrams in order to determine the fraction of solidified phases and the precipitation sequence at those particular compositions. For example, for the AlSi5Fe0.2Mn0.2 specimen, we analyzed the compositions AlSi3.17Fe0.29Mn0.18 (measured at position 3.1 mm) and AlSi8.26Fe0.14Mn0.23 (coordinate 7.8 mm). The specific compositions were selected to represent the extremes of solidification behavior possible within each sample.

For all specimens (five alloys) and all twenty-two measured compositions, phase mass fraction diagrams were calculated in Thermo-Calc (labeled in the software as “property diagrams”). These phase mass fraction diagrams (called in current study also phase fraction diagrams) were applied to create 2D maps. Each map presents mass fraction of precipitating phases including β -Al₅FeSi, Al₁₅Si₂Mn₄ and α -Al dendrites as a function of longitudinal position, which shows both the temperature of phase precipitation and general shape and density of the mushy zone. Considering each of the twenty-two points and processing them as a separate alloy with its own composition, the phase fraction diagrams were linked to a position on the longitudinal section (across the specimen diameter). This linking method is shown on Figure 2, where green arrow (diagram’s axis) moved from diagram was placed in chosen position together with phases fraction course (red and blue courses). EDS measurements were performed on rectangle areas with length and width of about 0.36 mm and placed side by side, at distances of 0.36 mm. The values of mass fraction from the phase fraction diagrams were transformed using graphical software into 0.36 mm wide belts and positioned side by side with 0.36 mm spacing. The length of 0.36 mm wide belts was determined by temperature range and oriented along the temperature axis on samples longitudinal section (Figure 2b). Knowing the solidification velocity (0.04 mm/s) and Artemis-3’s construction based on a linear temperature field, it was possible to transform temperature into length. Based on thermal macro-scale modeling, of course it would also be possible to apply nonlinear temperature field, and make similar plots. The 2D maps presenting mass fraction of the three solid phases as a function of location across the sample and temperature (or sample length) were prepared for each specimen, based on data included in phase fraction diagrams (Figure 2). The rescaling of temperature axis into a length axis was possible thanks to controlled solidification conditions (front velocity and temperature gradient) in the applied Bridgman-type furnace, and allowed preparation of 2D maps of the mushy zone.

Thermo-Calc [17] was used to calculate ternary phase diagrams (Figures 3 and 4) as liquidus projections by interval 2 °C for temperature range 550–900 °C. Phase fraction diagrams (Figures 2 and 5, Figures 6 and 7) were prepared by interval 2 °C and mass fraction interval 0.00017–0.00148 (for β -Al₅FeSi), 0.00017–0.00148 (for Al₁₅Si₂Mn₄), 0.017–0.059 (for α -Al) and 0.017–0.059 (for liquid).

3. Results

The five samples of nominal compositions described above were processed in Artemis-3 facility with intensive stirring generated by RMF. Fluid flow caused characteristic microstructure features previously found in alloys of AlSiMg [24], AlSiCu, [25], AlSiFe [21,26–28], Pb-Sn [29], and Sn-Cd [30], where segregation of elements, modification of dendrites or specific location of precipitate might be observed. Chemical compositions across each processed sample were precisely measured and those compositions were located on the Al-Si-Fe, Al-Si-Mn and Al-Fe-Mn ternary diagrams. The precipitation sequence was investigated for chosen points on the cross-section based on phase fraction diagrams. For each alloy, 2D maps presented mass fraction of occurring phases in the mushy zone.

3.1. Precipitation Sequence

The solidification reactions for the five nominal compositions follow the same order. First, a primary phase grows and it has a composition differing from the liquid. During the precipitation of primary phase, the liquid enriches in alloying elements and moves in the direction of binary eutectic mono-variant lines.

When the liquid reaches a mono-variant line, a binary eutectic starts to form. The range for binary eutectics formation in quaternary alloys is situated over a range of temperatures and compositions. The final liquid freezes when the composition reaches a three-phase eutectic point. In details for chosen two alloys, the solidification follows below presented precipitation sequence.

The predicted behavior of the AlSi5Fe0.2Mn0.2 specimen is given by the phase fraction diagram in Figure 2a, where α -Al starts to form first at 902.0 K (628.9 °C), in accordance with the reaction $L \rightarrow \alpha\text{-Al} + L$. On further cooling, the melt enriches in Si, Fe and Mn and at temperature 855.9 K (582.8 °C) the intermetallic phase $\text{Al}_{15}\text{Si}_2\text{Mn}_4$ starts to grow ($L \rightarrow \alpha\text{-Al} + \text{Al}_{15}\text{Si}_2\text{Mn}_4 + L$). At the point where $\text{Al}_{15}\text{Si}_2\text{Mn}_4$ appears, the mass fraction of α -Al dendrites has reached $f_\alpha = 0.64$. At temperature 848.0 K (574.9 °C) the AlSi eutectic begins to form; mass fraction reaches $f_\alpha = 0.68$ for α -Al and $f_{\text{Mn}} = 0.0019$ for $\text{Al}_{15}\text{Si}_2\text{Mn}_4$. Formation of the eutectic ($L \rightarrow \alpha\text{-Al} + \text{Al}_{15}\text{Si}_2\text{Mn}_4 + \text{Si} + L$) continues until 847.7 K (574.6 °C) when $\beta\text{-Al}_5\text{FeSi}$ starts to grow. The mass fraction of dendrites has now reached $f_\alpha = 0.95$, $f_{\text{Mn}} = 0.0105$ and AlSi eutectic mass fraction $f_{\text{Si}} = 0.0341$. The final solidification reaction $L \rightarrow \alpha\text{-Al} + \text{Al}_{15}\text{Si}_2\text{Mn}_4 + \beta\text{-Al}_5\text{FeSi} + \text{Si}$ occurs at 847.6 K (574.5 °C) when the mass fraction of the iron intermetallic phase has reached $f_\beta = 0.00136$. The equilibrium concentrations continue to change in the solid state, so that at room temperature (293.1 K/20.0 °C) the values have reached $f_\alpha = 0.937$, $f_{\text{Mn}} = 0.0065$, $f_{\text{Si}} = 0.0486$ and $f_\beta = 0.00757$.

For the specimen AlSi5Fe1.0Mn0.4 (Figure 2a), first α -Al forms at 899.9 K (626.8 °C) according to the reaction $L \rightarrow \alpha\text{-Al} + L$. At temperature 893.2 K (620.1 °C) $\text{Al}_{15}\text{Si}_2\text{Mn}_4$ intermetallic starts to grow ($L \rightarrow \alpha\text{-Al} + \text{Al}_{15}\text{Si}_2\text{Mn}_4 + L$) and the dendrite mass fraction has reached $f_\alpha = 0.182$. Next starts to precipitate $\beta\text{-Al}_5\text{FeSi}$ at temperature 867.8 K (594.7 °C) according to $L \rightarrow \alpha\text{-Al} + \text{Al}_{15}\text{Si}_2\text{Mn}_4 + \beta\text{-Al}_5\text{FeSi} + L$ and mass fraction for α -Al reaches $f_\alpha = 0.556$ and for $\text{Al}_{15}\text{Si}_2\text{Mn}_4$ $f_{\text{Mn}} = 0.0249$. The final eutectic reaction $L \rightarrow \alpha\text{-Al} + \text{Al}_{15}\text{Si}_2\text{Mn}_4 + \beta\text{-Al}_5\text{FeSi} + \text{Si}$ occurs at 847.6 K (574.5 °C) and mass fractions reach $f_\alpha = 0.923$, $f_{\text{Mn}} = 0.0240$, $f_{\text{Si}} = 0.0296$ and $f_\beta = 0.0235$. Mass fractions at temperature 293.1 K (20.0 °C) reach $f_\alpha = 0.902$, $f_{\text{Mn}} = 0.0129$, $f_{\text{Si}} = 0.0456$ and $f_\beta = 0.0367$. From Figure 2a, it can be concluded significant changes to the solidification behavior and phase precipitation can result from even small composition changes.

As described, melt stirring generated during processing caused segregation on the cross-section. The various local compositions (as in Figure 1b) were plotted on the three relevant ternary phase diagrams: Al-Si-Fe (Figure 3a), Al-Si-Mn (Figure 3b) and Al-Fe-Mn (Figure 4). The axes were set to 0–15% Si and 0–2% or 0–4% for Fe and Mn. These scales were small enough to permit spacing between points to be visible while also incorporating nearly all of the measured values. On the specimen AlSi5Fe1.0Mn0.4, which showed significantly more variability than the others, one point had a particularly high concentration of alloying elements (5.2% Si, 4.4% Fe and 1.2% Mn) and was excluded from the diagrams. On the Al-Fe-Mn diagram, where both axes were limited to 2%, a few additional measurements fell slightly outside the plotted area. These values are included along the edges of the graph with labels giving the true compositions. For selected measured compositions with particularly high or low Si, Fe and Mn content, phase fraction diagrams were prepared in order to assess solidification sequence (Figures 5–7) and these differ from sequences for the specimens' nominal compositions.

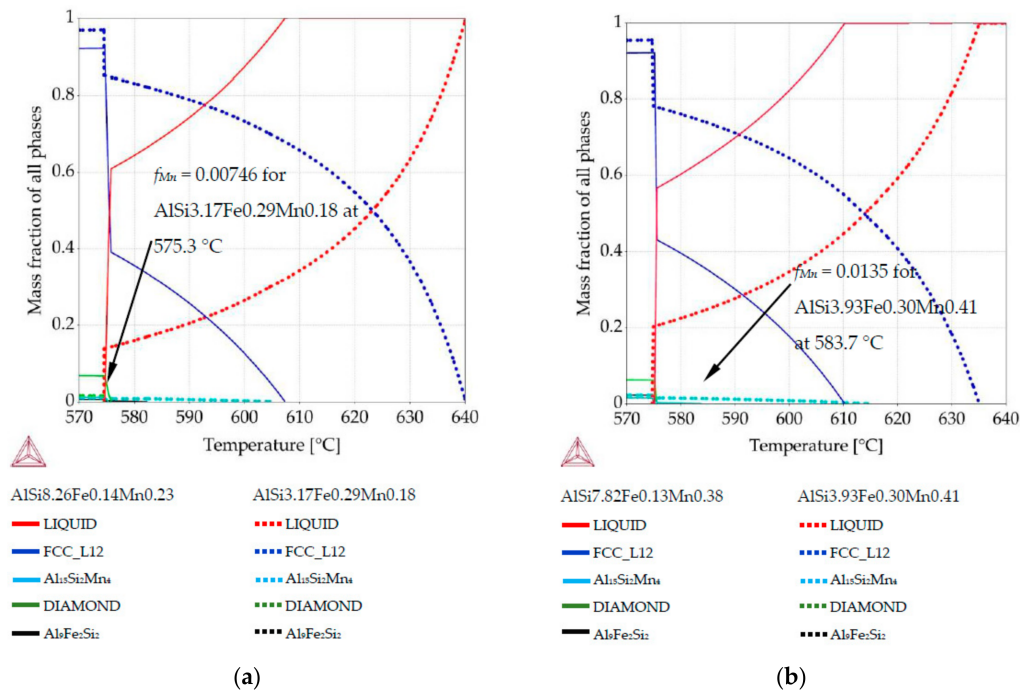


Figure 5. Phase mass fraction diagrams: (a) sample AlSi5Fe0.2Mn0.2, data for points with compositions AlSi8.26Fe0.14Mn0.23 and AlSi3.17Fe0.29Mn0.18; (b) sample AlSi5Fe0.2Mn0.4, data for points with compositions AlSi7.82Fe0.13Mn0.38 and AlSi3.93Fe0.30Mn0.41.

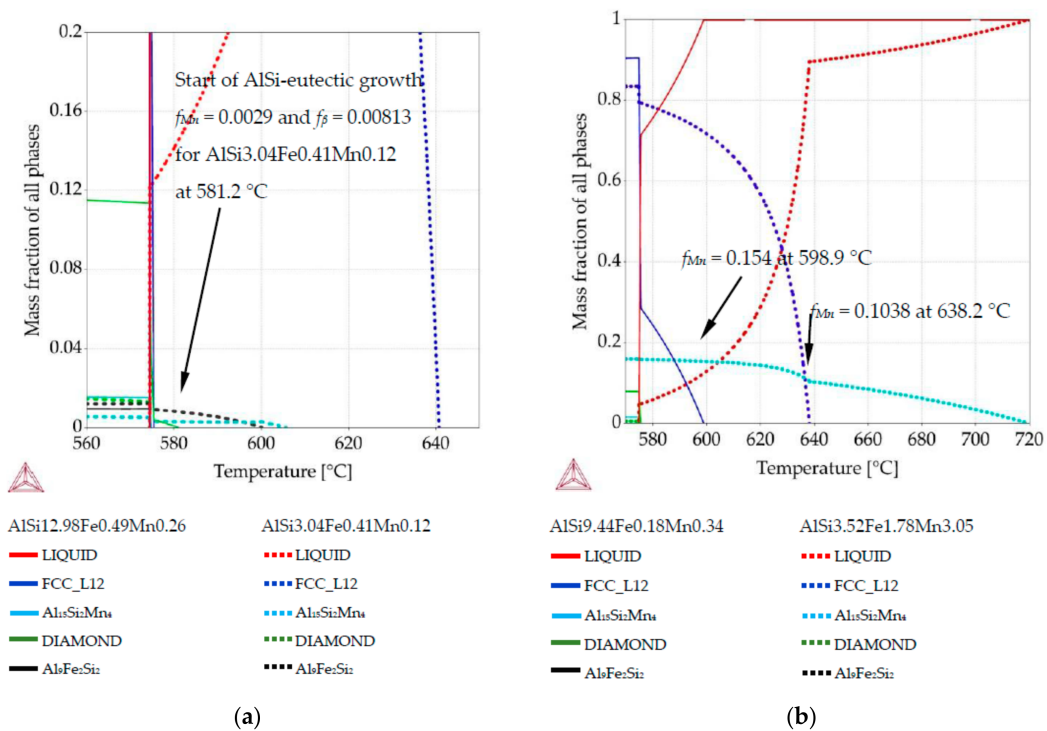


Figure 6. Phase mass fraction diagrams: (a) sample AlSi5Fe0.4Mn0.2, data for points with compositions AlSi12.98Fe0.49Mn0.26 and AlSi3.04Fe0.41Mn0.12; (b) sample AlSi5Fe0.4Mn1.0, data for points with compositions AlSi9.44Fe0.18Mn0.34 and AlSi3.52Fe1.78Mn3.05.

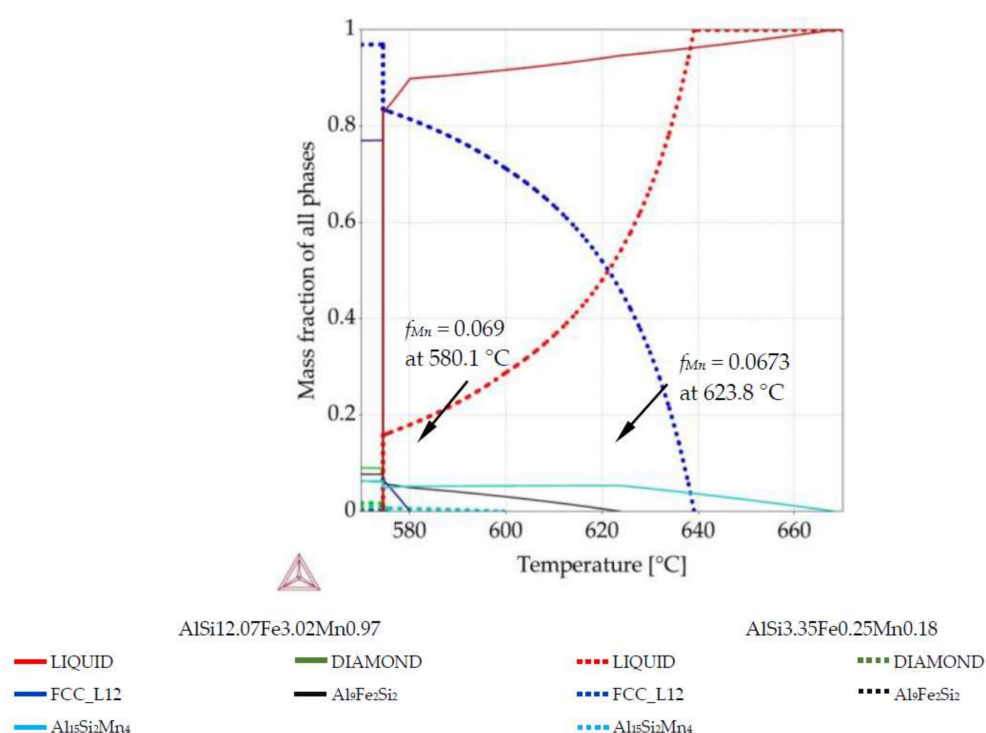


Figure 7. Phase mass fraction diagram for sample AlSi5Fe1.0Mn0.4, data for points with compositions AlSi12.07Fe3.02Mn0.97 and AlSi3.35Fe0.25Mn0.18.

There are some limitations to looking at the behavior of a quaternary alloy on a ternary phase diagram. However, a preliminary evaluation of the precipitation sequence of phases can still be carried out. On the three phase diagrams (Figures 3 and 4), the five nominal compositions are marked with filled shapes and the measured compositions marked with the corresponding open shape. For nominal composition AlSi5Fe0.2Mn0.2 (labeled as filled brown rhombus) the measured compositions (open brown rhombuses) are all placed in the compositional region where α -Al dendrites form as the first phase. The same is true for the AlSi5FeMn0.4 specimen; both nominal and all measured compositions indicate α -Al as the primary phase. The location of brown rhombuses and green squares indicates that the second phase may be AlSi eutectic, because for low Fe and Mn, the solidification paths moves direction eutectic groove where AlSi-eutectic forms ($L \rightarrow \alpha\text{-Al} + \text{Si} + L$ on Figure 3a,b). The AlSi5Fe0.4Mn0.2 specimen (labeled as blue triangles) also appears predominately in the α -Al region, but in this case three points were measured which had enough Si that primary Si or AlSi eutectic may appear first. On the specimen with nominal composition AlSi5Fe0.4Mn1.0 (labeled as red circles), the measured compositions are mainly located in the primary α -Al area, but a significant number (9 points out of 22) are observed where Al₁₅Si₂Mn₄ might appear first. In the specimen AlSi5Fe1.0Mn0.4 (violet octagons), a higher degree of scatter was observed. The measured compositions are still mainly located in the α -Al region, but in five points the first precipitate is likely to be β -Al₉Fe₂Si₂ or α -Al₈Fe₂Si and two other points have Si content near the eutectic composition.

3.2. Phase Mass Fraction Diagrams

Phase mass fraction diagrams (Figures 5–7) showing mass fraction of precipitating phases as a function of temperature were prepared for selected and mentioned above compositions. From the various compositions measured across the diameter of each sample, two composition values were selected which were thought to represent the biggest difference in precipitation sequence and characteristic temperature. On each diagram, solid lines are used for one of the measurements while dotted lines are used for the other. Figure 5a shows clearly that for the specimen AlSi5Fe0.2Mn0.2 the

variation in composition leads to a large difference in liquidus temperature: 607.3 °C at the point with composition AlSi8.26Fe0.14Mn0.23 (sample coordinate 3.1 mm; solid lines) and 640.1 °C for the point with composition AlSi3.17Fe0.29Mn0.18 (coordinate 7.8; dotted lines). For the high silicon composition, the precipitation of Al₁₅Si₂Mn₄ phase starts at 575.3 °C and reaches mass fraction $f_{Mn} = 0.011$ at 574.6 °C and finally $f_{Mn} = 0.0077$ at room temperature, compared to the low silicon composition, where Al₁₅Si₂Mn₄ appears at 604.6 °C and reaches $f_{Mn} = 0.009$ at final 574.5 °C and $f_{Mn} = 0.0064$ at temperature 20 °C. β -Al₅FeSi starts to grow in the mushy zone at 582.3 °C only for the second (low Si) composition; in the first composition the β phase appears only after all liquid is gone. At 20 °C, β mass fraction reaches $f_{\beta} = 0.0055$ for the high Si composition and $f_{\beta} = 0.0111$ for the low Si.

A similar situation is observed for the specimen AlSi5Fe0.2Mn0.4 (Figure 5b) where the liquidus temperature reaches 610.2 °C at the point with composition AlSi7.82Fe0.13Mn0.38 (coordinate 3.1 mm) and 635.1 °C for the point with composition AlSi3.93Fe0.30Mn0.41 (coordinate 6.0 mm). The precipitation of Al₁₅Si₂Mn₄ phase starts at 583.7 °C for the first composition and reaches mass fraction $f_{Mn} = 0.015$ at 575.1 °C, increasing to $f_{Mn} = 0.0130$ at room temperature. For the second composition, Al₁₅Si₂Mn₄ starts at 614.5 °C and reaches $f_{Mn} = 0.0221$ at 574.6 °C and finally $f_{Mn} = 0.0140$ at room temperature. At 20 °C, β -Al₅FeSi mass fraction reaches $f_{\beta} = 0.0049$ and $f_{\beta} = 0.0113$ respectively.

For the specimen AlSi5Fe0.4Mn0.2 (Figure 6a) variations in composition across the specimen caused not just different characteristic temperatures but also a change in precipitation sequence. At the point with very low Si content (AlSi3.04Fe0.41Mn0.12, coordinate 5.6 mm), the first phase to grow is dendritic α -Al, beginning at 640.7 °C, with the mass fraction reaching $f_{\alpha} = 0.969$ at final solidification temperature 574.5 °C. The precipitation of Al₁₅Si₂Mn₄ phase starts at 574.8 °C for the high silicon point, reaching $f_{Mn} = 0.0154$ at 574.5 °C and finally $f_{Mn} = 0.0088$ at room temperature. The low silicon composition begins to form Al₁₅Si₂Mn₄ starts at 605.7 °C and reaches $f_{Mn} = 0.0052$ at 574.5 °C and finally $f_{Mn} = 0.0042$ at room temperature. β -Al₅FeSi appears as part of the final solidification reaction at 574.5 °C for the composition AlSi12.98Fe0.49Mn0.26, but at 600.1 °C for AlSi3.04Fe0.41Mn0.12 and reaches $f_{\beta} = 0.0123$ at 574.5 °C. The opposite behavior is observed for the point with very high Si content (AlSi12.98Fe0.49Mn0.26, coordinate 4.5 mm) where the first phase to grow is AlSi eutectic, starting at 581.2 °C and where it is main and predominant phase in such the alloys. At 20 °C, β mass fraction reaches $f_{\beta} = 0.0182$ for AlSi12.98Fe0.49Mn0.26 and $f_{\beta} = 0.0154$ for AlSi3.04Fe0.41Mn0.12.

For the specimen with nominal composition AlSi5Fe0.4Mn1.0, the first phase to grow is Al₁₅Si₂Mn₄ (Figure 6b). The same precipitation sequence happens at the point with composition AlSi3.52Fe1.78Mn3.05, Mn-rich phases start to precipitate at 719.8 °C and reach mass fraction $f_{Mn} = 0.15973$ at final temperature 574.8 °C. However, at the point with composition AlSi9.44Fe0.18Mn0.34, Al₁₅Si₂Mn₄ starts to grow only at the final temperature 574.5 °C and reaches $f_{Mn} = 0.01577$. α -Al dendrites start to precipitate as the second phase at 638.2 °C at the point with the composition AlSi3.52Fe1.78Mn3.05 and mass fraction reaches $f_{\alpha} = 0.8351$ at final 574.5 °C, while dendrites are the first phase at the point with the composition AlSi9.44Fe0.18Mn0.34 and start at 598.9 °C and mass fraction reaches $f_{\alpha} = 0.9052$ at final 574.5 °C. At 20 °C, β -Al₅FeSi mass fraction reaches $f_{\beta} = 0.05833$ for AlSi3.52Fe1.78Mn3.05 and $f_{\beta} = 0.00591$ for AlSi9.44Fe0.18Mn0.34. Final Al₁₅Si₂Mn₄ mass fraction reaches $f_{Mn} = 0.08849$ for AlSi3.52Fe1.78Mn3.05 and $f_{Mn} = 0.00976$ for AlSi9.44Fe0.18Mn0.34 at room temperature.

For AlSi5Fe1.0Mn0.4 (Figure 7), dendritic α -Al is the first phase to grow. The same order applies to this specimen at the point with the composition AlSi3.35Fe0.25Mn0.18, where α -Al start to precipitate at 639.1 °C and reaches mass fraction $f_{\alpha} = 0.839$ at final temperature 574.5 °C. Meanwhile, at the point with composition AlSi12.07Fe3.02Mn0.97 dendrites start to grow at only 580.1 °C and reach $f_{\alpha} = 0.072$ at 574.5 °C. Al₁₅Si₂Mn₄ is the second phase to grow at the point with the composition AlSi3.35Fe0.25Mn0.18 and starts to precipitate at 599.5 °C and reaches $f_{Mn} = 0.00933$ at 574.5 °C. Phase fraction diagram (Figure 7) for the point with composition AlSi12.07Fe3.02Mn0.97 shows Al₁₅Si₂Mn₄ starting to grow first at temperature 668.3 °C and mass fraction reaches $f_{Mn} = 0.069$ at 574.5 °C. The second phase to appear is β -Al₅FeSi at 623.8 °C, reaching $f_{\beta} = 0.07713$ at 574.5 °C, while at the point AlSi3.35Fe0.25Mn0.18 Fe-rich phases start to grow at 575.2 °C and reach $f_{\beta} = 0.00389$

at 574.5 °C. At 20 °C, β -Al₅FeSi mass fraction reaches $f_{\beta} = 0.00926$ for AlSi_{3.35}Fe_{0.25}Mn_{0.18} and $f_{\beta} = 0.11221$ for AlSi_{12.07}Fe_{3.02}Mn_{0.97}. Final Al₁₅Si₂Mn₄ mass fraction reaches $f_{Mn} = 0.00607$ for AlSi_{3.35}Fe_{0.25}Mn_{0.18} and $f_{Mn} = 0.03225$ for AlSi_{12.07}Fe_{3.02}Mn_{0.97} at room temperature.

3.3. 2D Maps of Mushy Zone

2D maps (Figures 8–12) were based on the phase mass fraction diagrams prepared for each measured composition (each of 22 points of EDS measurement). The calculated mass fractions were placed according to the position on the longitudinal sections and prepared in graphical software and presented mass fraction of α -Al, β -Al₅FeSi, and Al₁₅Si₂Mn₄ as a function of position across the sample and position along the solidification direction or temperature. As described above, controlled directional solidification enabled the transformation of the temperature axis into the length axis and creation the 2D maps as shown.

α -Al mass fraction f_{α} (Figure 8a) for specimen AlSi₅Fe_{0.2}Mn_{0.2} shows the mushy zone of about 20 mm length in the range from 575 °C to about 635 °C. The upper part of mushy (marked by dendrites tips) seems to be rough, with one central liquid channel and two smaller channels at coordinates 1 mm and 7 mm. The central channel reaches the temperature 608 °C for α -Al mass fraction $f_{\alpha} = 0.2$ while the smaller channels reach the temperature 610 °C and 622 °C for $f_{\alpha} = 0.2$. The area without dendrites in the center is 1.0 mm wide at the bottom and 4 mm on top. β -Al₅FeSi (Figure 8b) starts to precipitate both in the center and in the outside part of specimen at about 575 °C, and only at one point (coordinate 7.5 mm) seems to start at about 580 °C. The final microstructure solidified at 575 °C is not richer in β -Al₅FeSi in the center (mass fraction about $f_{\beta} = 0.07$), which does not agree with earlier measurements of length L_{β} and number density n_{β} [21] of β -Al₅FeSi phases or with earlier similar assessment of mushy for AlSiFe alloys [31]. Solidification range for Al₁₅Si₂Mn₄ is about 575–600 °C (Figure 8c) and e.g., mass fraction $f_{Mn} = 0.004$ reached the temperature 600 °C only in two points (coordinate 1 mm and 7.5 mm). Over most of the area, Mn-phases precipitate at the final solidification temperature 575 °C. The final solidified microstructure shows almost equal mass fraction $f_{Mn} = 0.004$ –0.016 of Al₁₅Si₂Mn₄ and only in one point (coordinate 1 mm) is it increased to $f_{Mn} = 0.018$. In the AlSi₅Fe_{0.2}Mn_{0.2} specimen, Fe- and Mn-phases precipitate after α -Al dendrites close to 575 °C, and two points where Mn-phases start at 600 °C are placed by highly developed dendrites. The central liquid channel seems to be free of Fe- and Mn-rich phases.

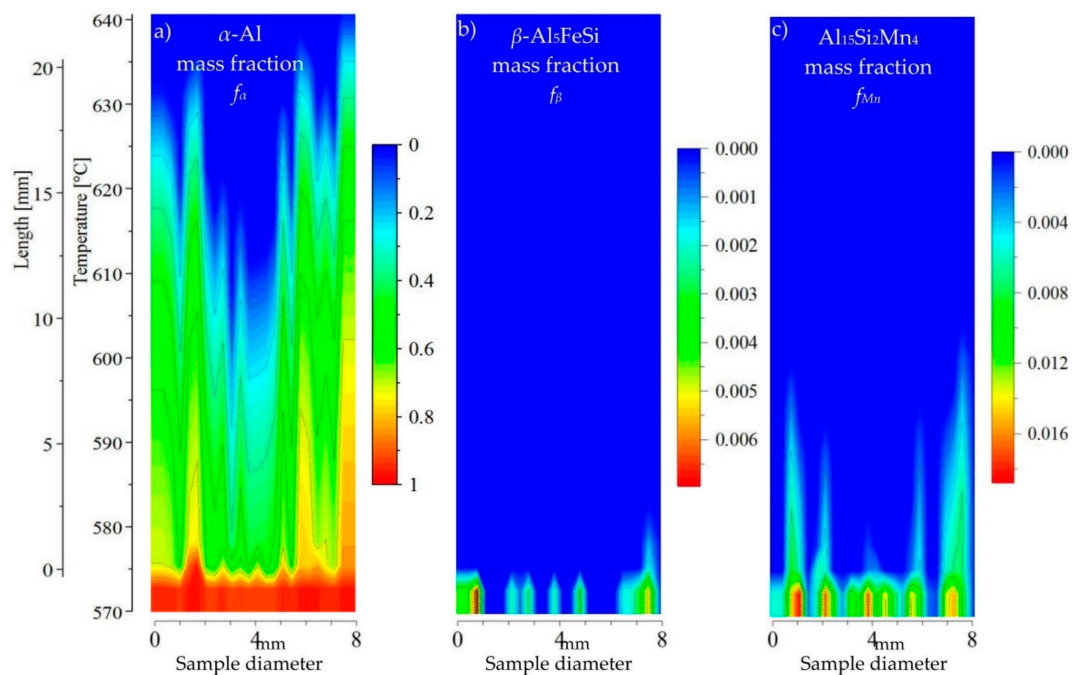


Figure 8. 2D maps showing phases mass fraction on longitudinal AlSi5Fe0.2Mn0.2 sample section: (a) α -Al mass fraction f_α ; (b) β -Al₅FeSi mass fraction f_β ; (c) Al₁₅Si₂Mn₄ mass fraction f_{Mn} .

For the specimen AlSi5Fe0.2Mn0.4, α -Al mass fraction f_α (Figure 9a) shows a liquid channel in the center, 4 mm wide on top at 625 °C and with rough 2 mm wide bottom at the temperature 602 °C (mass fraction $f_\alpha = 0.2$). The mushy zone seems to range from 575 °C to about 630 °C, and its length is about 17 mm. β -Al₅FeSi (Figure 9b) starts to precipitate at about 575 °C and only in one central point (coordinate 4.5 mm) with mass fraction reaching only about $f_\beta = 0.0016$. This location in the center agrees qualitatively with the central enrichment in Fe-phases in [21]. The solidification range for Al₁₅Si₂Mn₄ is about 575–610 °C (Figure 9c) and e.g., mass fraction $f_{Mn} = 0.01$ reached the temperature 605 °C in one point (coordinate 4.5 mm), but also in other points Mn-phases start to precipitate before the solidification temperature 575 °C. The final microstructure shows almost equal mass fraction $f_{Mn} = 0.015$ – 0.025 of Al₁₅Si₂Mn₄ and only in one point (coordinate 4.5 mm) it increased to $f_{Mn} = 0.036$. At this point, which has composition AlSi7.6Fe0.57Mn0.55, the temperature for starting of Al₁₅Si₂Mn₄ growth may even reach 610 °C, which coincides with a low α -Al mass fraction. It therefore seems as if some Mn-phases may nucleate and flow in the liquid channel, but the presence of β -Al₅FeSi seems to be impossible.

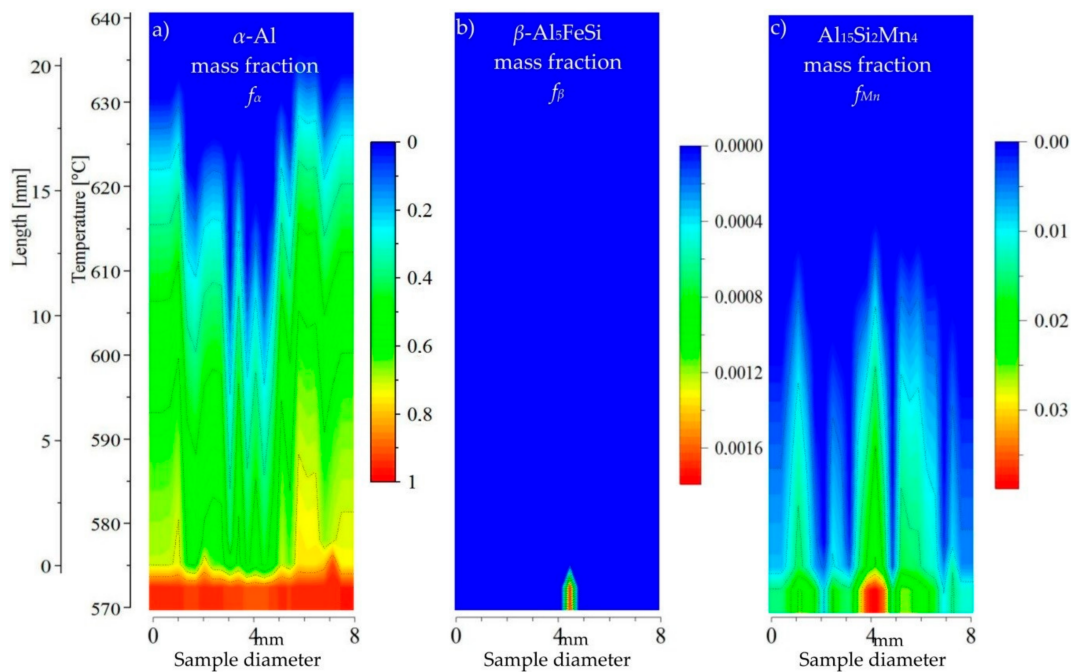


Figure 9. 2D maps showing phases mass fraction on longitudinal AlSi5Fe0.2Mn0.4 sample section: (a) α -Al mass fraction f_α ; (b) β -Al₅FeSi mass fraction f_β ; (c) Al₁₅Si₂Mn₄ mass fraction f_{Mn} .

Dendrite mass fraction f_α (Figure 10a) for specimen AlSi5Fe0.4Mn0.2 shows the mushy zone in temperature range from 575 °C to about 638 °C, with length of about 21 mm. The upper part of mushy marked by dendrites tips looks to be rough, but there is one clearly formed deep central channel. The liquid channel reaches the temperature 575 °C for α -Al mass fraction $f_\alpha = 0.2$ and is about 2.0 mm wide in the bottom at 575 °C and 3 mm on top at 635 °C. β -Al₅FeSi (Figure 10b) starts to precipitate across almost the whole specimen at about 575 °C, and only in three points with coordinate 1.5, 5.5 and 6.5 mm seems to start in the mushy zone, at about 598, 595 and 594 °C respectively. At the fourth point (coordinate 3.5 mm) Fe-phases start to grow at 582 °C and only at this one position coincide with the liquid channel. The final microstructure, frozen at 575 °C, is richer in the center in β -Al₅FeSi ($f_\beta = 0.018$) and agrees with earlier measurements [21] but generally mass fraction is low ($f_\beta = 0.010$). Solidification range for Al₁₅Si₂Mn₄ is about 575–600 °C and e.g., mass fraction $f_{Mn} = 0.004$ reached temperature 600 °C at several points (e.g., 3.2 mm and 6.2 mm). In half of the mushy zone located in the center, Mn-phases form at final solidification temperature 575 °C. Only one point (coordinate 3.5 mm) coincides with the liquid channel, where Mn-phases start to grow at 602 °C and it may be supposed that in liquid channel Al₁₅Si₂Mn₄ together with β -Al₅FeSi nucleate and freely flow. In the center, the microstructure is richer in Mn containing Al₁₅Si₂Mn₄ phase ($f_L = 0.020$) in comparison to external part ($f_L = 0.010$).

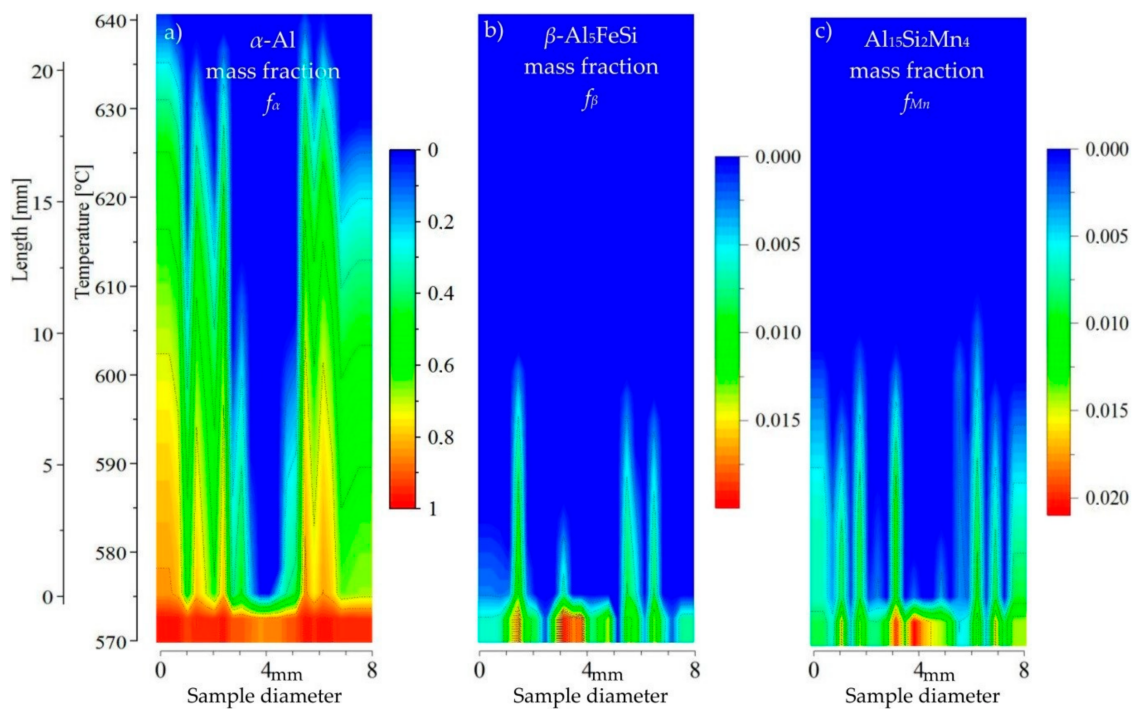


Figure 10. 2D maps showing phases mass fraction on longitudinal AlSi5Fe0.4Mn0.2 sample section: (a) α -Al mass fraction f_{α} ; (b) β -Al₅FeSi mass fraction f_{β} ; (c) Al₁₅Si₂Mn₄ mass fraction f_{Mn} .

α -Al mass fraction f_{α} (Figure 11a) for AlSi5Fe0.4Mn1.0 shows the mushy zone in the temperature range from 575 °C to about 640 °C, and its length is about 22 mm. The upper part of mushy zone (marked by dendrites tips) looks to be rough, with one central channel. The channel reaches the temperature 575 °C for α -Al mass fraction $f_{\alpha} = 0.2$. The dendrite-free area in the center is about 0.5 mm wide at 575 °C (bottom part) and 4 mm at 635 °C (top part) by $f_{\alpha} = 0.2$, and is much narrower than for the specimens described above. β -Al₅FeSi (Figure 11b) precipitates in very small amounts. The course of mass fraction for Al₁₅Si₂Mn₄ (Figure 11c) seems to be very specific. The solidification range for Al₁₅Si₂Mn₄ is about 575–710 °C and e.g., mass fraction $f_{Mn} = 0.004$ reached temperature 710 °C in two points (coordinates 4.0 mm and 5.5 mm), and in the third point (coordinate 1.5 mm) reached 640 °C. At other points Mn-phases start to grow near to final solidification temperature. In the mentioned three points the mass fraction amounts to about 0.08 or even 0.16 (for coordinate 5.5 mm). For Al₁₅Si₂Mn₄ the mass fraction varies across specimen. The starting temperature for Mn-phases in all three points is much higher than for dendrite tips, meaning that the Mn-phases may nucleate, grow and flow not only in liquid channel. The liquid area seems to be empty of Fe-phases.

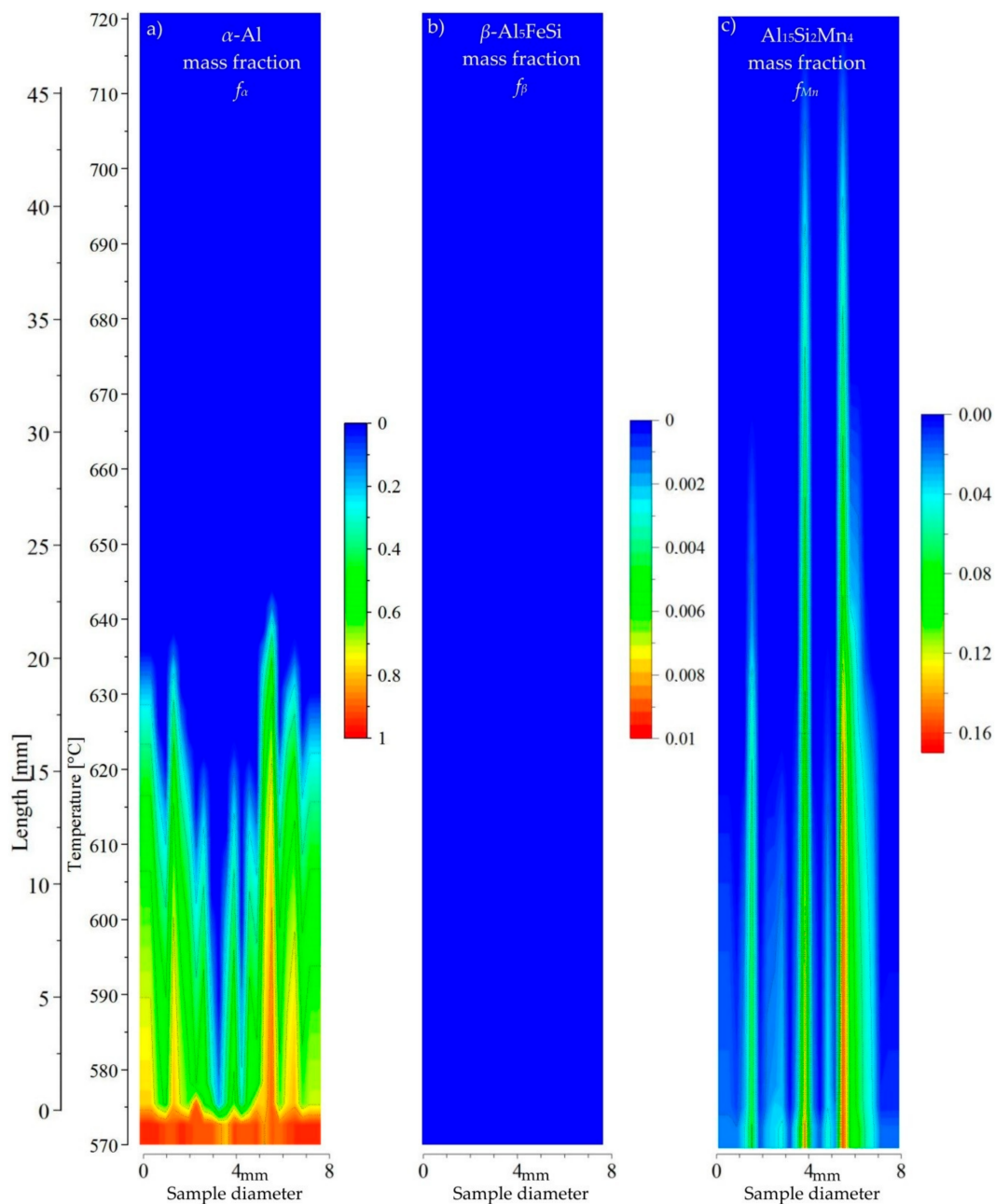


Figure 11. 2D maps showing phases mass fraction on longitudinal AlSi5Fe0.4Mn1.0 sample section: (a) α -Al mass fraction f_α ; (b) β -Al₅FeSi mass fraction f_β ; (c) Al₁₅Si₂Mn₄ mass fraction f_{Mn} .

For the specimen AlSi5Fe1.0Mn0.4 α -Al mass fraction f_α (Figure 12a) shows the mushy zone from 575 °C to about 635 °C, and about 20 mm long. The dendrite tips form rather rough profile (upper part of mushy) but there is one clearly formed deep central channel. The central channel reaches temperature 575 °C for α -Al mass fraction $f_\alpha = 0.2$. The dendrites free area in the center is 0.8 mm wide in the bottom at 575 °C and 2 mm on top at 620 °C. Solidification range for β -Al₅FeSi (Figure 12b) is about 575–605 °C and at points with coordinate 3.5, 4.5 and 5.5 mm β mass fraction $f_\beta = 0.02$ reaches the temperature 605 °C. At the other points Fe-phases precipitate almost at the final solidification temperature 575 °C. The final microstructure in the center is enriched in β -Al₅FeSi (mass fraction about $f_\beta = 0.11$) and corresponds to earlier measurements of length L_β and number density n_β [21] of β -Al₅FeSi phases and with earlier similar assessment of mushy for AlSiFe alloys [31]. The solidification range for Al₁₅Si₂Mn₄ is about 575–700 °C and e.g., mass fraction $f_{Mn} = 0.004$ reached temperature

700 °C in the point with coordinates 4.0 mm, about 670 °C at the second one (4.5 mm) and at the third point 620 °C (5.0 mm). These temperatures are all higher than the temperature of the dendrite tips. At the other points Mn-phases start to grow near to final solidification temperature. In the two points mentioned the mass fraction amounts about 0.16 or 0.11 (for coordinate 4.0 and 4.5 mm). The fully frozen microstructure in the center is richer in Mn-phases ($f_{Mn} = 0.10$) in comparison to external part ($f_{Mn} = 0.02$). At two points Mn-phases precipitate above dendrites and also at two central points Fe-phases start to grow before the dendrites tips. The liquid channel seems to be filled with β and $Al_{15}Si_2Mn_4$, and additionally in the area above the dendrites $Al_{15}Si_2Mn_4$ phases may nucleate and flow. Final microstructure for $AlSi_5Fe1.0Mn0.4$ can be seen on Figure 13, where the distribution of phases seems to coincide with predictions on 2D maps.

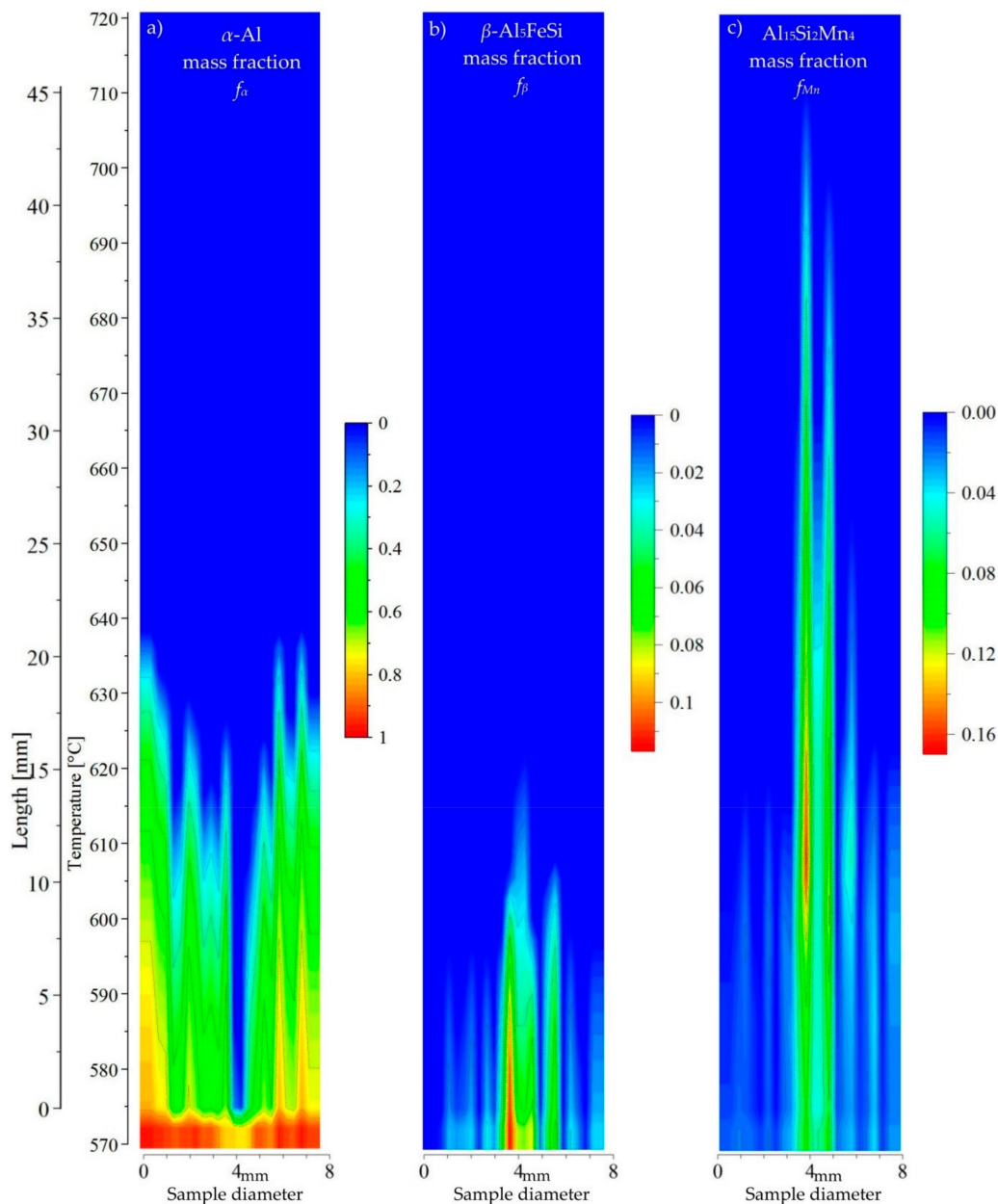


Figure 12. 2D maps showing phases mass fraction on longitudinal $AlSi_5Fe1.0Mn0.4$ sample section: (a) α -Al mass fraction f_{α} ; (b) β - Al_5FeSi mass fraction f_{β} ; (c) $Al_{15}Si_2Mn_4$ mass fraction f_{Mn} .

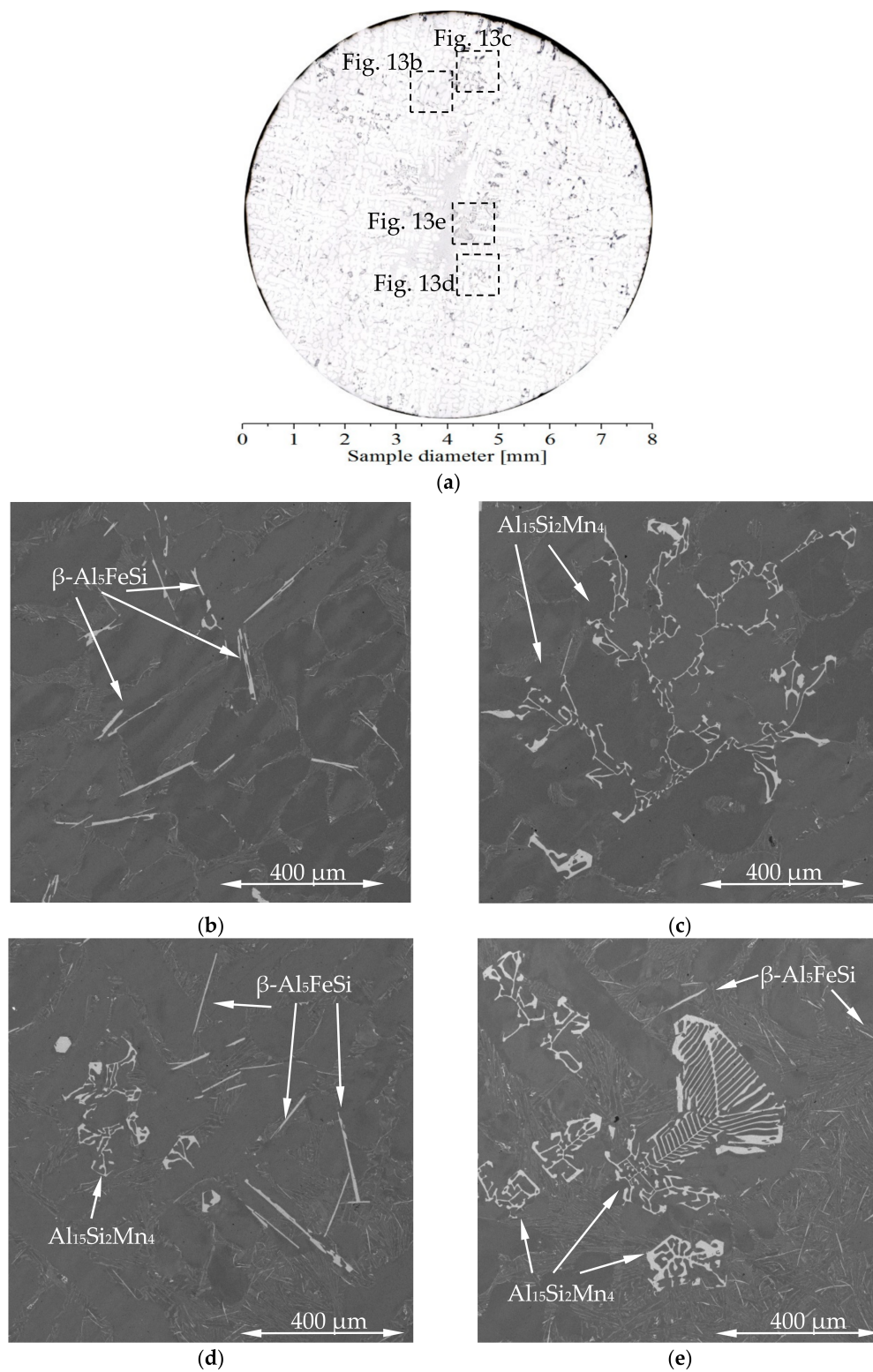


Figure 13. Specimen of Al-5 wt. % Si-1.0 wt. % Fe-0.4 wt. % Mn alloy: (a) a cross-sectional microstructure; (b) β - Al_5FeSi needle Fe-rich phases in dendritic area; (c) $\text{Al}_{15}\text{Si}_2\text{Mn}_4$ Mn-rich phases in dendritic area ; (d) β - Al_5FeSi needle Fe-rich phases in eutectic center ; (e) $\text{Al}_{15}\text{Si}_2\text{Mn}_4$ Mn-rich phases in eutectic center.

In studied specimens, the results achieved can be summarized as follow: melt stirring generated with rotating magnetic field produced changes in: (a) precipitation sequence; (b) characteristic temperatures of phases formation; (c) shape of mushy zone, i.e., formation of liquid channel; (d) mushy zone length; (e) movement of precipitating phases or deformation of dendritic structure, i.e., flow of Fe- or Mn phases in liquid channel or between dendrites and dendrites ripening or bending.

4. Discussion

In materials science the application of phase diagrams and phase mass fraction diagrams is very broad, however, this utilization of phase fraction diagrams is a new application, which seems to supply interesting information on the course of solidification.

The depiction of the mushy zone shown in the 2D maps (Figures 8–12) results from chemical composition mostly solidified at 575 °C and resulting from Si, Fe and Mn release by intensive stirring (RMF). The real structures are likely to differ slightly from what is shown in the figures. Nevertheless, the technique is able to provide some insight otherwise unavailable into the solidification process.

The use of aerogel as a crucible allowed the direct measurement of the intensity of radiation from samples' surface. Aerogel [19,32] is a transparent materials with very low thermal conductivity (5–20 mW/m·K). By using the recorded intensity, it was possibly to evaluate the intensity curves with characteristic peak-effect by solidus temperature and calculate directly the front velocity. Steinbach and Ratke [32] developed the method for mass fraction determination applicable in Artemis-3 but only for solidification with a planar front, without melt stirring. In the current study due to very small amounts of β -Al₅FeSi and Al₁₅Si₂Mn₄ and intensive stirring which disturbed the planar front, it was impossible to compare mass fraction of Fe- and Mn-intermetallics and also α -Al dendrites. The authors therefore decided to validate mass fraction according to simulation results [23].

Hainke [23] developed and applied simulation software for directional solidification with electromagnetic stirring. In calculations for AlSi7 ($G = 4$ K/mm, $B = 3$ mT) velocity isolines formed the deep area in the specimen center where isolines for mass fraction $f_L = 0.325$ descend 7.15 mm, showing a non-planar front. In [31] maps similar to those calculated in [23] were presented with 12–15 mm deep liquid channel in an AlSi7Fe1.0 alloy and for AlSi7Fe0.5 the depth reached 9–13 mm. Study [33] (specimen AlSi7Mn1.0) showed 13 mm long α -Al area and liquid channel (575–615 °C) and 28 mm long area (575–660 °C) for Al₁₅Si₂Mn₄ with Mn-phases growing above dendrites and in the channel. Current results conducted for 5% Si are similar to [31,33] for the same Si content (AlSi5Fe1.0 and AlSi5Mn0.2/0.4/1.0 respectively) with all showing a liquid channel where the α -Al dendrite area was about 20 mm long (575–635 °C).

For the AlSi5Fe0.2Mn0.2 specimen (Figure 8), the 2D maps showed precipitation of β -Al₅FeSi and Al₁₅Si₂Mn₄ after the α -Al dendrites, where Mn-phases appeared second and Fe-rich phases third near temperature 575 °C. The liquid channel, reaching 600 °C in length, and the liquid area above the dendrite tips seems to be empty of intermetallics. In the AlSi5Fe0.2Mn0.4 (Figure 9) as well, dendrites start to grow first, but only in a narrow area of the liquid channel (600 °C) may Al₁₅Si₂Mn₄ precipitate in small amount. The presence of Mn has reduced the precipitation of β and Mn-rich phases at least in the liquid channel. For AlSi5Fe0.4Mn0.2 (Figure 10) the growth area of the dendrites is longer than for β -Al₅FeSi and Al₁₅Si₂Mn₄ but with a wide and deep liquid channel. In that liquid channel Fe- and Mn-phases precipitate before dendrites, and it seems that they flow and may reach the liquid area above dendrites. For the AlSi5Fe0.4Mn1.0 (Figure 11) specimen, 1% of manganese has strongly reduced precipitation of β -Al₅FeSi and caused earlier precipitation of Mn-phases. At three points, Al₁₅Si₂Mn₄ precipitates before the dendrites in the liquid channel as well as above the α -Al, and intermetallic phases may freely flow in the liquid area. For AlSi5Fe1.0Mn0.4 (Figure 12), in the specimen center Mn-phases precipitate first in the liquid channel formed by the α -Al dendrites; the β phase regions appear second. In this way, Mn-phases may flow above the dendrites tips and in liquid channel Fe- and Mn-phases form, with the possibility of flowing into the liquid area above the α -Al dendrites.

The possibility of Fe- or Mn-phases moving through the liquid depends strongly on the morphology and dimension of intermetallic Fe- and Mn-phases, and the differences in the shape are well visible on Figure 13. Iron intermetallics form platelets [22] with various dimensions from a few micrometers to 1 mm, while Mn-rich phases [34] may take a shape ranging from compacted cubes (100 μm) to a large complex colony of cubes reaching above 1 mm. The fluidity of the solidifying melt might be decreased by the growth of other phases, e.g., Mg_2Si in Mg containing alloys [35]. In current study by $G = 3 \text{ K/mm}$, $v = 0.04 \text{ mm/s}$ and cooling rate $R = 0.12 \text{ K/s}$ only crystalline phases are considered, but flow conditions can change significantly by glassy structure for some alloys like $\text{Pd}_{40}\text{Cu}_{30}\text{Ni}_{10}\text{P}_{20}$ [36], where by also lower cooling rate (0.016 K/s, Table 4 in [36]) amorphous phases can precipitate. Amorphous structure is the domain of highly undercooled bulk glassy complex alloys, but surprising also possible to obtain even with only two elements e.g., $\text{Zr}_{65}\text{Ni}_{35}$ [37,38].

In previous papers predictions of the mushy zone have been presented for AlSiFe [31] and AlSiMn [33] alloys. The comparison of the AlSi5Fe1.0 (Figure 11 in [31]) and AlSi5Mn1.0 (Figure 11 in [33]) showed that by the same 1% amount of Fe or Mn, $\beta\text{-Al}_5\text{FeSi}$ may precipitate only in the liquid channel (Figure 11 in [31]), while $\text{Al}_{15}\text{Si}_2\text{Mn}_4$ may precipitate in the liquid channel and above dendrites tips (Figure 11 in [33]). Similar observations apply to AlSi7Fe1.0 (Figure 12 in [31]) and AlSi7Mn1.0 (Figure 12 in [33]) only with a shorter mushy zone. The addition of Mn to AlSi5Fe1.0 (Figure 11 in [31]) caused the formation of $\text{Al}_{15}\text{Si}_2\text{Mn}_4$ (Figure 12, specimen AlSi5Fe1.0Mn0.4) in the liquid channel and between dendrites, while the area of $\beta\text{-Al}_5\text{FeSi}$ and $\alpha\text{-Al}$ are parallel. The comparison of AlSi5Mn0.2 (Figure 9 in [33]) and AlSi5Fe0.2Mn0.2 (Figure 8) showed that the addition of 0.2% Fe has not caused the formation of a significant amount of β because of the reduction in manganese. The formation of Mn-phases is similar in both specimens, but the dendritic area does not form such clear liquid channel (Figure 9 in [33]) as in AlSi5Fe0.2Mn0.2 (Figure 8).

The sample with AlSi5Fe0.4Mn0.2 (Figure 10) in comparison to AlSi5Mn0.2 (Figure 9 in [33]) showed this time that the addition of 0.4% Fe is enough to form β phases and $\text{Al}_{15}\text{Si}_2\text{Mn}_4$ and due to the presence of the liquid channel, the flow of both intermetallics in channel and above the dendrites is possible. In AlSi5Mn0.2 (Figure 9 in [33]) Mn phases form as the second phase between $\alpha\text{-Al}$, and intermetallics do not flow in liquid area. In the specimens AlSi5Mn1.0 (Figure 11 in [33]) and AlSiFe0.4Mn1.0 (Figure 11) the growth area for $\alpha\text{-Al}$ dendrites has a similar temperature range (575–640 $^\circ\text{C}$) and liquid channel. The addition of 0.4% Fe in the presence of 1% Mn has caused the formation of a very small amount of $\beta\text{-Al}_5\text{FeSi}$. Manganese intermetallics precipitate in both specimens in the liquid channel and high above the dendrite tips. The presence of iron has caused the temperature range for $\text{Al}_{15}\text{Si}_2\text{Mn}_4$ growth to be about 710 $^\circ\text{C}$ for AlSi5Fe0.4Mn1.0 and 670 $^\circ\text{C}$ for AlSi5Mn1.0 (Figure 11 in [33]), but the amount of intermetallics is smaller.

The mushy zone length varies according to the composition. The dendritic area is about 20 mm (575–635 $^\circ\text{C}$) long for all specimens, but the whole predicted mushy zone differs according to Fe and Mn content. According to [39], the flow by rotating electromagnetic field 3 mT in axial direction may enclose the mushy length on 12 mm and flow velocities in axial direction 2.5 mm/s, while in the current experiment the applied field of 6 mT may cause a velocity of 10.5 mm/s. It seems that these velocities concern only about 12 mm area, but the flow generated by the field also propagates outside it and may cause stirring in that region. There is no indication that increased flow velocities and more intensive rotation (of liquid alloy and flowing solid precipitates) resulting from increased field strength (from 3 to 6 mT) may point on the longer area with included stirring.

In our analysis we considered there to be a fixed composition along the sample length, and of course the changes occurring across sample diameter presented by EDS measurements. However, fluid flow may change composition due to segregation. The almost constant chemical composition along sample length in similar studies [40] was presented for AlSi7Fe1.0 alloy (120 mm long and 8 mm diameter specimens) solidified directionally without stirring. The segregation was found both across and along the sample for experiments with temperature gradient 7 K/mm and high rotating magnetic field (HRMF) of 150 mT. From the specimen beginning (coordinate 1 mm, 2.5 wt. % Si and 0.6 wt. % Fe),

the amount of alloying elements increased almost linearly to the sample end (coordinate 100 mm, 12.8 wt. % Si and 1.7 wt. % Fe). Considering similar changes, by the length of our dendritic area (about 20 mm), between 575 °C isoline and dendrite tips, the Si content might increase to about 1.2 wt. %. Such changes might move the composition on the Al-Si-Fe (Figure 3a) or on the Al-Si-Mn (Figure 3b) phase diagram (Figure 3) to the right, and the 7 °C decrease of liquidus and might cause dendrites to be about 2.3 mm shorter and the liquid channel to be slightly wider. Because solidification by HRMF [40] were carried out with 150 mT and current studies by RMF only 6 mT, it can be stated that results presented here would be much less than a 10% reduction, as an effect of segregation across the sample diameter.

The main cause for the liquid channel is segregation of Si and results are similar to [23,31,33]. The segregation of Mn and Fe is not so uniform as in Fe-containing AlSi alloys [31]. Specimens with iron and manganese show slightly irregular values across the sample, with some enrichment in the center (e.g., AlSi5Fe1.0Mn0.4), but also near the outside (e.g., AlSi5Fe0.2Mn0.2). The morphologies of platelet-shaped β -Al₅FeSi and complex Mn-rich intermetallics seems to be the primary factor influencing the enrichment in the center and some outside [34]. α -Al dendrites form a skeleton structure with a liquid channel in the center. By the time the mass fraction reaches about $f_{\alpha} = 0.9$, the dendrites may stay fixed in the fully solidified bottom part of the specimen and not move. Fe- and Mn-phases with dimensions about 0.001–2 mm and mass fraction 0.0–0.15 do not form an immovable structure. Especially the results for Mn-phase precipitating above the dendrites tips and seen on the 2D map figures as high vertical pillars, present only a probability of the intermetallics location and not the stable frame. The shape, density and location of phases (α -Al, β , Al₁₅Si₂Mn₄) are factors strongly determining permeability of mushy zone and the fluid flow that occurred should be analyzed carefully.

5. Conclusions

Phase mass fraction diagrams created in Thermo-Calc were used to investigate the effect of segregation on the sequence of phase precipitation and the characteristic temperatures within specimens of AlSi alloys with Fe- and Mn-rich phases. Phase fraction diagrams presenting the mass fraction of phases were utilized to produce 2D maps and provide an efficient visualization method for directionally solidified alloys.

The two-dimensional maps presented spatial orientation and value of phases mass fraction (α -Al dendrites, β -Al₅FeSi, Al₁₅Si₂Mn₄) occurring in the mushy zone. The calculations showed the center of the mushy zone occupied by a liquid channel that sometimes reaches deep into the mushy zone until a solidification temperature around 575 °C. This channel is caused mainly by Si segregation. The mushy zone may reach above α -Al dendrites because of Mn-rich phases starting to form at higher temperatures. The liquid channel may remain empty of β -Al₅FeSi and Al₁₅Si₂Mn₄ phases, or the Fe- and Mn-phases may nucleate and freely flow in the liquid channel and over the dendrites tips. Al₁₅Si₂Mn₄ phases may precipitate at higher temperatures than β and may reach a higher mass fraction in liquid melt.

The specimen centers showed enrichment in AlSi eutectic for all alloys as in previous studies, but for β -Al₅FeSi and Al₁₅Si₂Mn₄ the results are ambiguous. In some specimens β and Mn-rich phases showed a higher mass fraction in the center, both at the final solidification temperature and above it, which agrees with earlier studies. However, in some other specimens the mass fraction varies across the samples and does not show the enrichment of Fe- and Mn-phases or elements in the center. Fe-phases start to grow mainly at temperatures below the dendrites and in this way may flow in general between them. Mn-rich phases start to precipitate in higher temperatures than β and in many places before α -Al, in this way flowing in the liquid melt above the mushy zone. It seems that this movement in the liquid above the dendrites allows the Mn-rich phases to be located in various places across the specimen, while β may favor the specimen center. The predicted formation of high vertical pillars of Al₁₅Si₂Mn₄ phases indicate growth probability and not solid stable frame.

Acknowledgments: The research leading to these results has received funding from the People Programme (Marie Curie Actions) of the European Union's Seventh Framework Programme (FP7/2007-2013) under Research Executive Agency REA grant agreement No. PCIG13-GA-2013-613906.

Author Contributions: Piotr Mikolajczak designed and performed experiments. Piotr Mikolajczak performed thermodynamic calculations, prepared diagrams and conceived the idea of 2D maps, analyzed experimental and numerical data and wrote the paper. Amber Genau and Piotr Mikolajczak analyzed results and wrote the manuscript. Amber Genau contributed correction of English and proofreading. Jerzy Janiszewski evaluated the rotating magnetic field. Lorenz Ratke contributed consultation. All authors reviewed the final paper and contributed substantially to the work reported.

Conflicts of Interest: The authors declare no conflict of interest. The funding sponsor is the European Union's Seventh Framework Programme (FP7/2007-2013). The founding sponsors had no role in the design of the study; in the collection, analyses, or interpretation of data; in the writing of the manuscript, and in the decision to publish the results.

References

1. Massalski, T.B.; Okamoto, H. *Binary Alloy Phase Diagrams*; ASM International: Geauga County, OH, USA, 1990; ISBN 978-0871704030.
2. Kaufman, L.; Bernstein, H. *Computer Calculation of Phase Diagrams with Special Reference to Refractory Metals*; Academic Press: New York, NY, USA, 1970; ISBN 9780124020504.
3. Lukas, H.; Fries, S.G.; Sundman, B. *Computational Thermodynamics—The Calphad. Method*; Cambridge University Press: Cambridge, UK, 2007; ISBN 978-0-521-86811.
4. Hillert, M. *Phase Equilibria, Phase Diagrams and Phase Transformations—Their Thermodynamic Basis*; Cambridge University Press: Cambridge, UK, 1998; ISBN 978-0-521-85351-4.
5. Shi, P.; Sundman, B. *Thermo-Calc. Software System—Thermodynamic Framework and Data*; Thermo-Calc Software AB; Foundation of Computational Thermodynamics: Stockholm, Sweden, 2013.
6. Firouzdor, V.; Rajabi, M.; Nejati, E.; Khomamizadeh, F. Effect of microstructural constituents on the thermal fatigue life of A319 Al alloy. *Mater. Sci. Eng. A* **2007**, *454–455*, 528–535. [[CrossRef](#)]
7. Yi, J.Z.; Gao, Y.X.; Lee, P.D.; Lindley, T.C. Effect of Fe-content on fatigue crack initiation and propagation in a cast aluminium-silicon alloy (A356-T6). *Mater. Sci. Eng. A* **2004**, *386*, 396–407. [[CrossRef](#)]
8. Ma, Z.; Samuel, A.M.; Samuel, F.H.; Doty, H.W.; Valtierra, S. A study of tensile properties in Al-Si-Cu and Al-Si-Mg alloys. Effect of beta-iron intermetallics and porosity. *Mater. Sci. Eng. A* **2008**, *490*, 36–51. [[CrossRef](#)]
9. Kim, H.Y.; Han, S.W.; Lee, H.M. The influence of Mn and Cr on the tensile properties of A356-0.20Fe alloy. *Mater. Lett.* **2006**, *60*, 1880–1883. [[CrossRef](#)]
10. Hwang, J.Y.; Doty, H.W.; Kaufman, M.J. The effects of Mn additions on the microstructure and mechanical properties of Al-Si-Cu casting alloys. *Mater. Sci. Eng. A* **2008**, *488*, 496–504. [[CrossRef](#)]
11. Sreeja Kumari, S.S.; Pillai, R.M.; Pai, B.C. A study on the structural, age hardening and mechanical characteristics of Mn and Ca added Al-7Si-0.3Mg-0.6Fe alloy. *J. Alloys Compd.* **2008**, *453*, 167–173. [[CrossRef](#)]
12. Khalifa, W.; Samuel, F.H.; Gruzleski, J.E. Iron intermetallic phases in Al corner of the Al-Si-Fe system. *Metall. Mater. Trans. A* **2003**, *34*, 807–825. [[CrossRef](#)]
13. Bridgman, P.W. Certain physical properties of single crystals of tungsten, antimony, bismuth, tellurium, cadmium, zinc and tin. *Proc. Am. Acad. Arts Sci.* **1925**, *60*, 305–383. [[CrossRef](#)]
14. Stockbarger, D.C. The production of large single crystals of lithium fluoride. *Rev. Sci. Instrum.* **1936**, *7*, 133–136. [[CrossRef](#)]
15. Jung, H.; Mangelinck-Noël, N.; Nguyen-Thi, H.; Billia, B. Columnar to equiaxed transition during directional solidification in refined Al-based alloys. *J. Alloys Compd.* **2009**, *484*, 739–746. [[CrossRef](#)]
16. Ruvalcaba, D.; Mathiesen, R.H.; Eskin, D.G.; Arnberg, L.; Katgerman, L. In situ observations of dendritic fragmentation due to local solute-enrichment during directional solidification of an aluminum alloy. *Acta Mater.* **2007**, *55*, 4287–4292. [[CrossRef](#)]
17. Thermo-Calc 4.1—Software Package from Thermo-Calc Software AB, Stockholm, Sweden. Available online: www.thermocalc.se (accessed on 16 March 2015).
18. Alkemper, J.; Sous, S.; Stoker, C.; Ratke, L. Directional solidification in an aerogel furnace with high resolution optical temperature measurements. *J. Cryst. Growth* **1998**, *191*, 252–260. [[CrossRef](#)]
19. Steinbach, S.; Ratke, L. In situ optical determination of fraction solid. *Scr. Mater.* **2004**, *50*, 1135–1138. [[CrossRef](#)]

20. Steinbach, S. The Influence of Fluid Flow on the Microstructure Evolution of Directional Solidified Al-Si and A-Si-Mg Alloys. Ph.D. Thesis, Rheinisch-Westfälische Technische Hochschule (RWTH) Aachen University, Aachen, Germany, 28 November 2005. (In German)
21. Mikolajczak, P.; Ratke, L. Effect of stirring induced by rotating magnetic field on β -Al₅FeSi intermetallic phases during directional solidification in AlSi alloys. *Int. J. Cast Met. Res.* **2013**, *26*, 339–353. [[CrossRef](#)]
22. Mikolajczak, P.; Ratke, L. Interplay between melt flow and the 3D distribution and morphology of Fe-rich phases in AlSi alloys. *Metall. Mater. Trans. A* **2015**, *46*, 1312–1327. [[CrossRef](#)]
23. Hainke, M. Computation of Convection and Alloys Solidification with the Software Package CrysVUn. Ph.D. Thesis, Technical Faculty of Friedrich-Alexander Universität Erlangen-Nürnberg, Erlangen, Germany, July 2004.
24. Steinbach, S.; Ratke, L. The influence of fluid flow on the microstructure of directionally solidified AlSi-base alloys. *Metall. Mater. Trans. A* **2007**, *38*, 1388–1394. [[CrossRef](#)]
25. Steinbach, S.; Ratke, L. Experimental study on interaction of fluid flow and solidification in Al-Si-Cu alloys. *Int. J. Cast Met. Res.* **2007**, *20*, 140–144. [[CrossRef](#)]
26. Steinbach, S.; Euskirchen, N.; Witusewicz, V.; Ratke, L. Fluid flow effects on intermetallic phases in Al-cast alloys. *Trans. Indian Inst. Met.* **2007**, *60*, 137–141.
27. Kovacs, J.; Sveda, M.; Ronafoldi, A.; Roos, A. Influence of high rotating magnetic field (RMF) on the solidified structure of Al-7 wt. % Si-1 wt. % Fe alloy. In Proceedings of the 6th Decennial Conference on Solidification Processing, Beaumont Estate, Old Windsor, UK, 25–28 July 2017.
28. Budenkowa, O.; Nagy, C.; Du Terrail Couvat, Y.; Steinbach, S.; Roos, A.; Fautrelle, Y. Comparison of 2D and 3D simulations of solidification of binary and ternary Al-based alloys under RMF. In Proceedings of the 6th Decennial Conference on Solidification Processing, Beaumont Estate, Old Windsor, UK, 25–28 July 2017.
29. Kovacs, J.; Ronafoldi, A.; Roos, A. Unidirectional solidification of Pb-Sn alloys in a rotating magnetic field. *Mater. Sci. Forum* **2013**, *790–791*, 408–413. [[CrossRef](#)]
30. Sveda, M.; Sycheva, A.; Kovacs, J.; Ronafoldi, A.; Roos, A. The effect of rotating magnetic field on the solidified structure of Sn-Cd peritectic alloys. *Mater. Sci. Forum* **2013**, *790–791*, 414–419. [[CrossRef](#)]
31. Mikolajczak, P.; Ratke, L. Thermodynamic assessment of mushy zone in directional solidification. *Arch. Foundry Eng. AFE* **2015**, *15*, 101–109. [[CrossRef](#)]
32. Steinbach, S.; Ratke, L. In situ optical determination of fraction solid of Al-Si-Mg alloys. *Mater. Sci. Forum* **2006**, *508*, 491–496. [[CrossRef](#)]
33. Mikolajczak, P.; Genau, A.; Ratke, L. Mushy Zone Morphology Prediction with Application of CALPHAD Technique. *Metals* **2017**, *7*, 363. [[CrossRef](#)]
34. Mikolajczak, P.; Ratke, L. Three dimensional morphology of Mn rich intermetallics in AlSi alloys investigated with X-ray tomography. *Mater. Sci. Forum* **2014**, *790–791*, 335–340. [[CrossRef](#)]
35. Mikolajczak, P. Microstructural evolution in AlMgSi Alloys during solidification under electromagnetic stirring. *Metals* **2017**, *7*, 89. [[CrossRef](#)]
36. Inoue, A.; Takeuchi, A. Recent progress in bulk glassy alloys. *Mater. Trans.* **2002**, *43*, 1892–1906. [[CrossRef](#)]
37. Ghidelli, M.; Volland, A.; Blandin, J.-J.; Pardo, T.; Raskin, J.-P.; Momprou, F.; Djemia, P.; Gravier, S. Exploring the mechanical size effects in Zr₆₅Ni₃₅ thin film metallic glasses. *J. Alloys Compd.* **2014**, *615*, 90–92. [[CrossRef](#)]
38. Ghidelli, M.; Gravier, S.; Blandin, J.-J.; Pardo, T.; Raskin, J.-P.; Momprou, F. Compositional-induced structural change in Zr_xNi_{100-x} thin film metallic glasses. *J. Alloys Compd.* **2014**, *615*, 348–351. [[CrossRef](#)]
39. Hainke, M.; Friedrich, J.; Müller, G. Numerical study on directional solidification of AlSi alloys with rotating magnetic field under microgravity conditions. *J. Mater. Sci.* **2004**, *39*, 2011–2015. [[CrossRef](#)]
40. Roos, A.; Kovacs, J.; Ronafoldi, A.; Kovacs, A. Effect of high rotating magnetic field on the solidified structure of Al-7 wt. % Si-1 wt. % Fe alloy. *Mater. Sci. Forum* **2013**, *752*, 57–65. [[CrossRef](#)]

